


Neoclassical Tearing Mode Seeding by Nonlinear Three-Wave Interactions in Tokamaks

L. Bardóczy^{1,*}, N. C. Logan², and E. J. Strait¹¹General Atomics, P.O. Box 85608, San Diego, California 92186-5608, USA²Lawrence Livermore National Laboratory, Livermore, California 94551, USA (Received 17 March 2021; revised 26 May 2021; accepted 22 June 2021; published 30 July 2021)

We report the experimental observation of seed magnetic island formation by nonlinear three-wave coupling of magnetic island triplets. In this experiment, disruptive 2,1 islands are seeded by the coupling of 4,3 and 3,2 tearing modes to a central 1,1 sawtooth precursor. Three-wave interactions between these modes are conclusively identified by bispectral analysis, indicating fixed phase relationships in agreement with theory. This new observation of this seeding mechanism has important implications for future reactors that must operate in stable plasma equilibria, free of disruptive 2,1 islands.

DOI: 10.1103/PhysRevLett.127.055002

Introduction.—Nonlinear three-wave interaction is an important process in a number of fields within physics, for example, in nonlinear optics [1], in quantum mechanics [2], in hydrodynamics [3], and in plasma turbulence [4]. For example, in fluids and plasmas, this interaction leads to the cascade of quadratic invariants, resulting in universal scaling laws of fluctuation spectra [5]. Magnetic reconnection and three-wave interaction of magnetohydrodynamic (MHD) modes are topics of significant interest in the study of the magnetosphere, the ionosphere, and the solar wind [6], as well as in magnetic confinement fusion research, for example, between fast-ion modes [7]. The theory of nonlinear three-wave coupling applies to magnetic island triplets with the general matching conditions for wave vectors ($k_1 + k_2 = k_3$) and frequencies ($f_1 + f_2 = f_3$). In tokamaks, the wave vector equation is equivalent to matching conditions for poloidal (m) and toroidal (n) mode numbers $m_1 + m_2 = m_3$ and $n_1 + n_2 = n_3$ [8,9]. Magnetic islands are closed helical flux tubes formed by magnetic reconnection [10]. They are of strong interest in tokamak research, particularly the $m, n = 2, 1$ island, as it is the primary cause of rapid and violent discharge terminations, called disruptions [11]. This island is often formed by the pressure-gradient-driven neoclassical tearing mode (NTM), a nonlinear resistive MHD instability that requires a seed in order to grow. NTM seeds are known to be formed by transient events such as core-localized sawtooth crashes [12] and edge-localized modes (ELMs) [13]. However, nonlinear three-wave coupling of preexisting magnetic islands is a potential new type of NTM seeding in tokamaks. Tearing mode cascade [14] and magnetic island phase locking have been observed [15,16] in toroidal fusion devices. Magnetic island seeding by three-wave interactions was considered in Joint European Torus [17], but conclusive evidence has never

been reported, leaving this important prediction an open question for decades.

In this Letter we report conclusive experimental evidence of magnetic island seeding by nonlinear three-wave coupling in tokamaks for the first time. Of most importance, we report disruptive 2,1 NTM seed formation by 4,3 and 3,2 tearing mode (TM) interaction with a 1,1 sawtooth precursor in DIII-D plasmas [18] using the International Thermonuclear Experimental Reactor (ITER) baseline scenario's normalized parameters and shape [19].

Experimental setup.—The relevant parameters are as follows: 1.76 m magnetic axis major radius (R_0), 0.56 m minor radius (a), 1.35 MA plasma current (I_p), 1.8 T toroidal magnetic field (B_T), 4.6 MW neutral beam power, and no electron cyclotron heating. The EFIT [20] magnetic equilibrium is constrained by motional Stark effect spectroscopy [21] and by external magnetic probes [22]. The $q = 2$ surface is at $\rho \approx 0.73$ (ρ is the square root of the normalized toroidal flux, and q is the safety factor, the number of toroidal transits per single poloidal transit of a field line on a toroidal flux surface). The electron density (n_e) is $6 \times 10^{19} \text{ m}^{-3}$, and the electron temperature (T_e) is 1.2 keV (Thomson scattering [23]) at $q = 2$. The normalized plasma beta is near constant at 1.8 ($\beta_N = \beta a B_T / I_p$, where β is the ratio of plasma pressure to magnetic pressure). Because of the high density, the electron cyclotron emission (ECE) near $q = 2$ is absorbed; hence local measurements of the ECE electron temperature are not possible.

MHD instabilities are monitored via measurements of the poloidal magnetic field perturbation (\tilde{B}_θ) [22]. These sensors provide $5 \mu\text{s}$ temporal resolution, as well as mode number identification with $m \leq 5$, $n \leq 5$. \tilde{B}_θ of each TM opens a magnetic island structure where the mode helicity matches the equilibrium magnetic field helicity, at $q = m/n$. This results in m (n) islands in the poloidal (toroidal) plane.

As the island rotation is dominantly toroidal the island rotation frequencies are $f_{m,n}/n$, where $f_{m,n}$ are the measured magnetic fluctuation frequencies in the laboratory frame.

2,1 Island seeding by three-wave interactions.—In the analyzed discharges, viable 2,1 seed islands are produced by nonlinear three-wave coupling between phase-locked TMs. Seeding occurs either (i) when initially decoupled high m, n TMs grow to a sufficiently large amplitude, then slow down and nonlinearly couple to a 1,1 sawtooth precursor or (ii) when small-amplitude high m, n modes phase lock together at the 1,1 frequency for multiple sawtooth periods until one grows to a sufficiently large amplitude. Here we present an example of the first type.

The representative discharge in Fig. 1 is characterized by ELM events [shown in Fig. 1(a) by the spikes of D_α emission from the plasma edge] and sawtooth crash events [shown in Fig. 1(e) by the sudden cessation of the 1,1 precursor]. In the analyzed time frame, the plasma β is held constant, and the current profile has fully relaxed. This is seen from the fact that q_{95} (q at $\psi = 0.95$, ψ is the normalized poloidal flux), q_{\min} (minimum of q), and l_i (plasma internal inductance) are constant [Fig. 1(a)] and $j_{\parallel}(r)$ (parallel current density profile) is fixed (not shown).

The 2,1 seeding occurs at $t \approx 4721$ ms, which is marked by a vertical dashed line. There is no ELM [Fig. 1(a)], and there is no sawtooth crash [Fig. 1(f)] at this time either. Hence this 2,1 island is not seeded by an ELM or a sawtooth crash. Three modes participate in the 2,1 seeding: a 1,1 sawtooth precursor; a 4,3 island; and a 3,2 island. The \bar{B}_θ spectrogram in Fig. 1(b) shows that the 1,1 mode near the $f_{1,1} = 3.7$ kHz frequency grows and crashes periodically about every 75 ms. The 3,2 island rotates with a stable frequency near $f_{3,2} = 7.4$ kHz, and the 4,3 island slows from a maximum frequency of about $f_{4,3} = 14$ kHz to about 11 kHz by the time of the seeding event. $f_{1,1}$ at the 2,1 formation is marked by the lower horizontal dashed line. In addition, the second and third harmonic frequencies are also marked with dashed horizontal lines in Fig. 1(b). The 2,1 island forms when the 4,3 couples to the 3,2 and the 1,1, in agreement with the time histories of the $f_{m,n}/n$ rotation frequencies [Fig. 1(c)] and A_n magnetic amplitudes [Figs. 1(d) and 1(e)].

In accord with the spectrogram in Fig. 1(b), the frequency time traces in Fig. 1(c) show that the 1,1 and 3,2 modes are rotationally coupled to each other initially, but the 4,3 mode is not coupled to them. $f_{1,1}$ and $f_{3,2}$ are nearly constant (apart from small drops caused by ELMs) while the 4,3 island is slowing. This slowing is caused presumably by the electromagnetic torque between the 4,3 and 3,2 islands as their corresponding rational surfaces are only 4 cm apart. The torque from the 1,1 mode has a similar effect, while, with sufficiently high rotation frequency, the drag from induced wall currents remains relatively small. Figure 1(e) shows that the robust $n = 1$ growth begins when the 4,3 island couples to the 3,2 and 1,1 modes. At

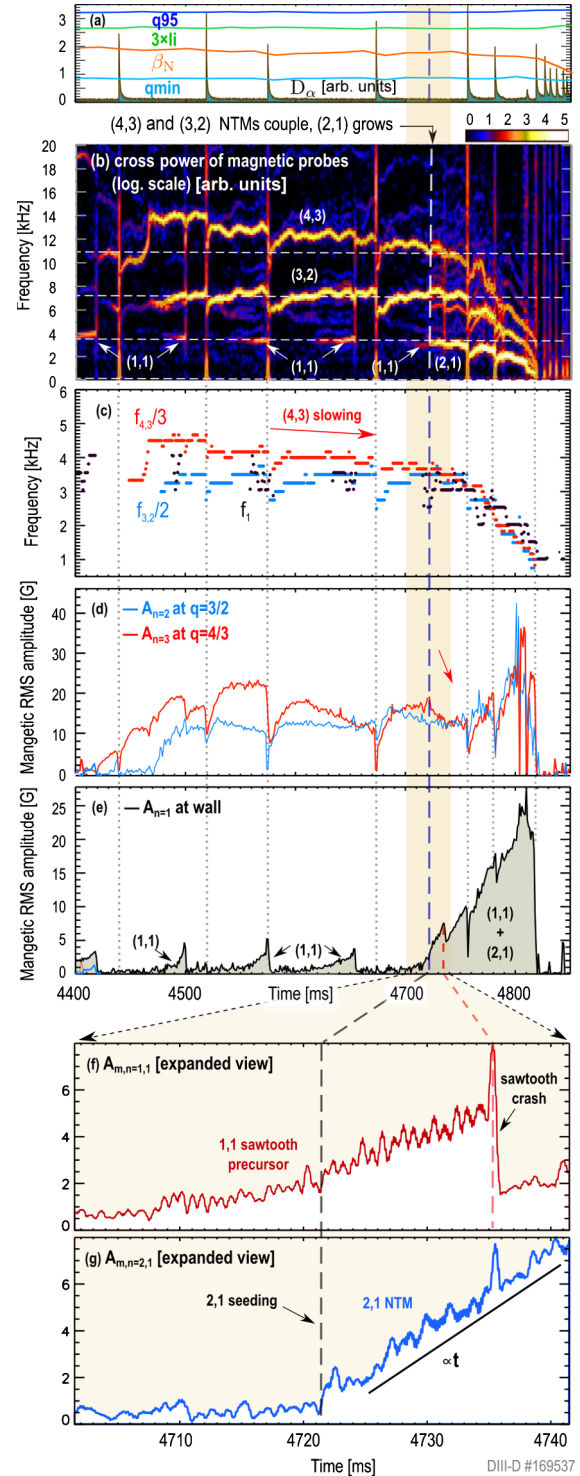


FIG. 1. (a) q_{95} , l_i , β_N , q_{\min} , and D_α . (b) Cross power spectrogram of \bar{B}_θ signals. (c) Frequency of $n = 1, 2$, and 3 modes. Magnetic amplitude of (d) $n = 2$ and 3 modes and (e) $n = 1$ mode. Expanded view of (f) 1,1 and (g) 2,1 amplitudes.

this time the $n = 1$ amplitude increases to about twice the amplitude of previous 1,1 modes [Fig. 1(e)], and the 4,3 amplitude rapidly decreases [Fig. 1(d)]. This is consistent with the 1,1 being driven by the coupling between the 4,3

and the 3,2, while the 1,1 and coupled 3,2 island produce the 2,1 seed island. These three-wave interactions satisfy the following relations at $f_{m,n}/n = \text{const}$:

$$(m, n = 4, 3) - (m, n = 3, 2) \rightarrow (m, n = 1, 1), \quad (1)$$

$$(m, n = 3, 2) - (m, n = 1, 1) \rightarrow (m, n = 2, 1). \quad (2)$$

Simultaneous measurements of \tilde{B}_θ in the high-field-side and low-field-side midplane enable isolation of the $m = 1$ and $m = 2$ components for the $n = 1$ signal. The 1,1 amplitude in Fig. 1(f) and the 2,1 amplitude in Fig. 1(g) show that at the time of 4,3 and 3,2 coupling the 1,1 amplitude is about 2 G and the 2,1 amplitude suddenly grows to about 2 G. The 1,1 mode does not crash at this time, clarifying that the 2,1 island is not seeded by a sawtooth crash. The 2,1 grows linearly in time, consistent with a neoclassically driven island, and the 1,1 crashes about 14 ms later (marked by the second vertical dashed line). Both the amplitude and lifetime of this sawtooth instability are consistent with the preceding 1,1 modes in the discharge. At the time of this crash the 2,1 amplitude is already about 6 G, and it continues to grow linearly thereafter, interrupted by small drops caused by ELMs. Note that the 2,1 field perturbation is about 1 G at the time of seeding, which is a very small fraction ($\approx 10^{-4}$) of the equilibrium field.

Phase locking.—While rotation-frequency matching is evident from the $f_{m,n}/n$ time traces in Fig. 1(c), fixed phase relationships are conclusively identified by bicoherence (b^2) analysis in Fig. 2(a). b^2 is the squared normalized bispectrum, which is a statistical measure for quantifying the extent of phase coupling between frequency pairs (f_1, f_2) in a single signal, often used to identify nonlinear interactions in measured data [24]. To reduce the statistical noise, b^2 is calculated from each of the 14 \tilde{B}_θ probes of the outboard midplane toroidal array separately in a 70 ms window around the time of seeding, then averaged between all probes:

$$b^2 = \left\langle \frac{|\langle F_{i,n}(f_1)F_{i,n}(f_2)F_{i,n}^*(f_1+f_2) \rangle_n|^2}{\langle |F_{i,n}(f_1)F_{i,n}(f_2)|^2 \rangle_n \langle |F_{i,n}^*(f_1+f_2)|^2 \rangle_n} \right\rangle_i. \quad (3)$$

Here $F_{i,n}$ is the Fourier transform of the n th segment in the i th magnetic probe data. \tilde{B}_θ is sampled at 200 kHz, giving 14 000 points in a 70 ms window. This allows one to divide each probe signal to 70 segments, with 200 points per segment. Here * stands for complex conjugate and $\langle \dots \rangle_n$ ($\langle \dots \rangle_i$) for averaging over the segments (probes). b^2 in Fig. 2(a) shows a fixed phase relationship between (i) the 4,3 and 3,2 frequencies at the time of seeding (approximately 11 and 7 kHz) and (ii) the 3,2 and $n = 1$ frequencies (approximately 7.0 and 3.5 kHz). The maximum value of $b^2(f_1, f_2)$ in these frequency bins is about

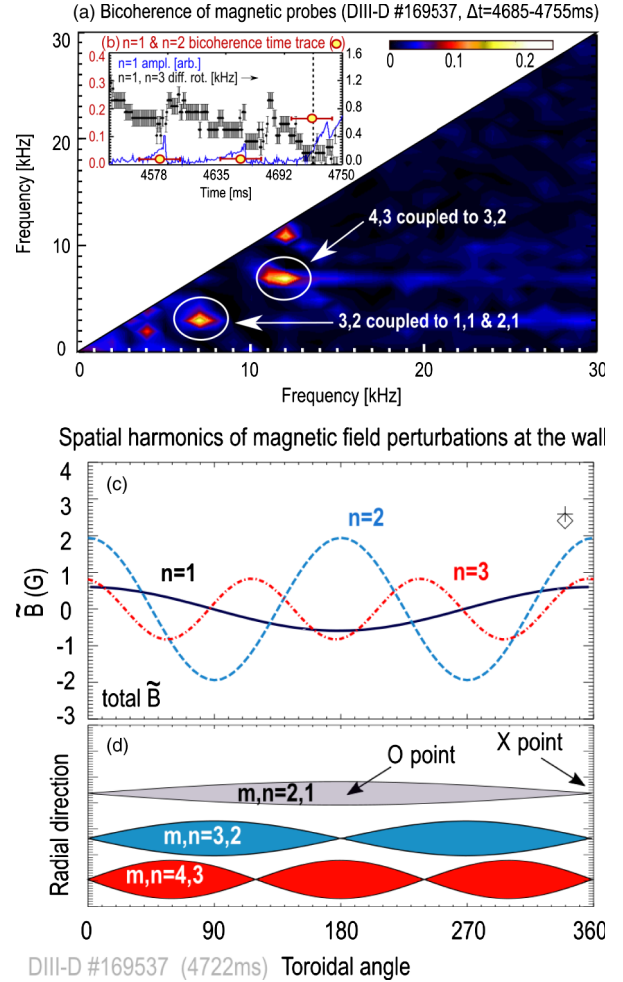


FIG. 2. (a) Bicoherence of \tilde{B}_θ at the time of 2,1 seeding. (b) Time trace of bicoherence between the $n = 1$ and $n = 2$ modes, $n = 1$ amplitude, and differential rotation of $n = 1$ and $n = 3$ modes. (c) Spatial harmonics of \tilde{B}_θ . (d) Cartoon of 2,1; 3,2; and 4,3 islands with phasing derived from (c).

23%, with a significance level of 2%. Note that $b^2(f_1, f_2)$ in these bins is comparable to the significance level before the seeding event, indicating that the 3,2 island is slowly drifting with respect to the 1,1 mode before the 4,3 island couples to them, as shown in Fig. 2(b). Therefore, there is no nonlinear three-wave interaction between the $n = 1$ and $n = 2$ modes until the 4,3 island couples. The fact that the rapidly rotating 4,3 island resides between the 1,1 and 3,2 modes offers an explanation for this observation.

Phase relationships.—The phases and amplitudes of the $n = 1, 2,$ and 3 harmonics are calculated by spatial Fourier decomposition of \tilde{B}_θ measured by the low-field-side midplane toroidal sensor array at an instant of time in the phase-locked state [25]. In these spatial harmonics, the m, n island X points (O points) correspond to the maxima (minima) of the corresponding n th harmonic. Figures 2(b) and 2(c) show that the phase-locked state is characterized by the alignment of one of the X points of the 2,1; 3,2; and

4,3 island chains in the outboard midplane (at $\phi = 0$ in this example), in agreement with theory [26].

Magnetic energy balance.—The 4,3 magnetic amplitude drops at the time of 2,1 seeding, while the 3,2 amplitude remains near constant [Fig. 1(d)]. This is consistent with the 4,3 magnetic energy converting to form the 2,1 seed, in accord with Eqs. (1) and (2). To estimate the energy balance, we adopt the $\tilde{B}_{\theta,m} = C_m m^{-1} (r/r_s^{m,n})^{(m+1)}$ at $r < r_s^{m,n}$ and $\tilde{B}_{\theta,m} = -C_m m^{-1} (r_s^{m,n}/r)^{(m+1)}$ at $r > r_s^{m,n}$ cylindrical model for the poloidal magnetic field perturbation of a TM [27]. The C_m amplitudes are constrained by the measurements of $\tilde{B}_{\theta,m}$ at the wall, and the resonant surface locations ($r_s^{m,n}$) by the EFIT. The magnetic energy of each mode is proportional to the $I_m = \int \tilde{B}_{\theta,m}^2 dV$ volume integral, which is evaluated separately for the 2,1 and 4,3 modes before and after the seeding event (at $t = 4721.5$ ms and $t = 4722.0$ ms, respectively). This simple model estimates that the drop of the 4,3 magnetic energy accounts for 96% of the 2,1 seed island magnetic energy.

Note that while the 4,3 and 3,2 amplitudes are relatively small at the wall, they are generally much larger in the core as (i) the tearing eigenfunctions peak where $q = m/n$ which are deeper for the 4,3 and 3,2 (compared with the 2,1) and (ii) they decay quicker with respect to r . Specifically, in this plasma, the maximum of the 3,2 (4,3) is 14% (9%) at the wall relative to the 25 G at which the 2,1 disrupted. Mapping \tilde{B}_{θ} to $q = m/n$ yields that the 3,2 (4,3) amplitude at the time of seeding is 34% (54%) at $q = 3/2$ ($q = 4/3$) with respect to the 2,1 amplitude at $q = 2$ at the time of disruption (≈ 35 G). The seed island produces a 1 G magnetic field at the probe, corresponding to 1.4 G at $q = 2$. This perturbation is smaller than the 4,3 and 3,2 amplitudes at $q = 2$. Therefore, these high m/n modes should not be discounted in the analysis and in the interpretation of the discharge evolution as the relative amplitudes at the wall are not proportional to those in the core.

Classical stability.—To evaluate classical stability, we calculated the ideal MHD $n = 1$ global stability parameter (δW) and the $m = 2$ diagonal element of the $n = 1$ Δ' matrix (Δ'_{22}) with STRIDE [28] in the 500 ms window prior to the 2,1 onset. STRIDE uses state transition matrix methods [29] to parallelize integrations of the Euler-Lagrange equation, reducing the extrema of the perturbed energy to a response matrix form $\delta W = (1/2\mu_0)\Xi^\dagger W \Xi$ as in DCON [30]. Here, Ξ is a vector of complex poloidal harmonic coefficients of the displacement at the plasma boundary, and μ_0 is the vacuum magnetic permeability. The lowest eigenvalue of this response matrix (δW_1) is shown in Fig. 3. Its constant, positive value indicates that energy is required to distort the plasma with $n = 1$ toroidal asymmetry (i.e. the plasma is stable to ideal MHD modes). The code also calculates a full toroidal Δ' matrix, an extension of the tearing parameter [31]. Figure 3 also shows Δ'_{22} (a representative matrix element, which would reduce to

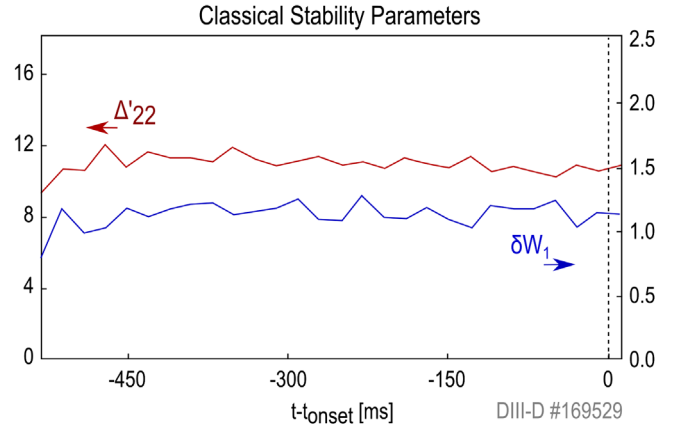


FIG. 3. δW_1 and Δ'_{22} . Positive values reflect stable conditions.

the classical Δ' in cylindrical geometry), which also stays approximately constant. This steady Δ' corresponds to a growth rate of roughly 550 s^{-1} according to RDCON [30]. Note that the coupling of the rational surfaces in toroidal geometry does result in a nondiagonal matrix here however, meaning the sign of this element is no longer intuitively indicative of the sign of the mode growth rate. δW and Δ'_{22} do not cross any threshold prior to the 2,1 growth, indicating no change in the classical tearing stability can explain the sudden growth of the experimentally observed mode.

Summary and discussion.—We reported the first observation of seed magnetic island formation by nonlinear three-wave coupling in tokamaks. We reported 2,1 seed island formation by 4,3 and 3,2 island interaction with a 1,1 sawtooth precursor in the DIII-D ITER baseline scenario. These 2,1 seeds rapidly grow and terminate the discharges. These plasmas reach the β and current flattop, and are robustly stable to classical tearing modes. A number of ELMs and sawtooth crashes undergo without seeding the 2,1 island in the absence of nonlinear three-wave coupling. Seeding occurs when high m, n islands couple at various times in the stationary plasma. The magnetic energy of the seed island accounts for the drop of the coupling modes' energy, and the seeded 2,1 island grows linearly thereafter in accord with neoclassical theory. Therefore, these observations clarify that magnetic reconnection at $q = 2$ is not caused by a classical current-driven instability, but the 2,1 NTM seed island is formed by frequency matching and nonlinearly interacting TMs that satisfy the mode number resonance condition. Three-wave interactions are conclusively identified with bispectral analysis, indicating fixed phase relationships at the time of 2,1 seeding. The phase-locked state is characterized by the alignment of one of the X points of the islands in the outboard midplane, as predicted. These results are general and relevant for future reactors, as 70% of the considered unstable DIII-D ITER baseline scenario discharges of the past decade without electron cyclotron current drive are characterized by frequency matching of resonant tearing modes at the time

of 2,1 island seeding. This mechanism is also a candidate to account for TM cascades, which has remained unexplained since its first observation in 1989 [14]. In the absence of the 1,1 mode, 2,1 seeding could most likely occur when, e.g., the 3,2's first (second) harmonic couples to the 5,3 (4,3). This implies that even if the sawtooth instability and ELMs are controlled, high m, n islands can nonlinearly interact to seed disruptive 2,1 islands. As the nonlinear three-wave interaction produces seed 2,1 islands while the plasma is robustly stable to classical tearing modes, tearing free operation may not be possible by locking in a classically stable current profile in future reactors. This predicts new challenges for the development of stable plasma scenarios, calling for active control, suppression, and avoidance of high m, n modes as much as possible.

The authors acknowledge very helpful discussions with Carlos A. Paz-Soldan, Richard Fitzpatrick, Zhirui Wang, and Jim D. Callen. This material is based upon work supported by the U.S. Department of Energy, Office of Science, Office of Fusion Energy Sciences, using the DIII-D National Fusion Facility, a DOE Office of Science user facility, under Award No. DE-FC02-04ER54698. This report was prepared as an account of work sponsored by an agency of the United States government. Neither the United States government nor any agency thereof, nor any of their employees, makes any warranty, express or implied, or assumes any legal liability or responsibility for the accuracy, completeness, or usefulness of any information, apparatus, product, or process disclosed, or represents that its use would not infringe upon privately owned rights. The views and opinions of authors expressed herein do not necessarily state or reflect those of the United States government or any agency thereof.

*bardoczil@fusion.gat.com

- [1] C. Li, *Optical Three-Wave Coupling Processes*, 978-981-10-1488-8 (Springer, Singapore, 2017).
- [2] M. Wadati and K. Ohkuma, *J. Phys. Soc. Jpn.* **53**, 1229 (1984).
- [3] R. A. Kraichnan, *Phys. Fluids* **10**, 1417 (1967).
- [4] A. Hasegawa and K. Mima, *Phys. Fluids* **21**, 87 (1978).
- [5] A. N. Kolmogorov, *Proc. R. Soc. A* **434**, 9 (1941).
- [6] M. Yamada, R. Kulsrud, and H. Ji, *Rev. Mod. Phys.* **82**, 603 (2010).
- [7] N. A. Crocker, W. A. Peebles, S. Kubota, E. D. Fredrickson, S. M. Kaye, B. P. LeBlanc, and J. E. Menard, *Phys. Rev. Lett.* **97**, 045002 (2006).
- [8] C. C. Hegna, *Phys. Plasmas* **3**, 4646 (1996).
- [9] R. M. Coelho, E. Lazzaro, M. F. Nave, and F. Serra, *Phys. Plasmas* **6**, 1194 (1999).
- [10] R. J. La Haye, *Phys. Plasmas* **13**, 055501 (2006).
- [11] P. C. de Vries, M. F. Johnson, B. Alper, P. Buratti, T. C. Hender, H. R. Koslowski, V. Riccardo, and J.-E. Contributors, *Nucl. Fusion* **51**, 053018 (2011).
- [12] V. Igochine, A. Gude, S. Günter, K. Lackner, Q. Yu, L. Barrera Orte, A. Bogomolov, I. Classen, R. M. McDermott, and N. C. Luhmann, *Phys. Plasmas* **21**, 110702 (2014).
- [13] R. J. La Haye, P. A. Politzer, and D. P. Brennan, *Nucl. Fusion* **48**, 015005 (2008).
- [14] E. J. Strait, L. L. Lao, A. G. Kellman, T. H. Osborne, R. Snider, R. D. Stambaugh, and T. S. Taylor, *Phys. Rev. Lett.* **62**, 1282 (1989).
- [15] S. Assadi, S. C. Prager, and K. L. Sidikman, *Phys. Rev. Lett.* **69**, 281 (1992).
- [16] B. Tobias, M. Chen, I. G. J. Classen, C. W. Domier, R. Fitzpatrick, B. A. Grierson, N. C. Luhmann, C. M. Muscatello, M. Okabayashi, K. E. J. Olofsson *et al.*, *Phys. Plasmas* **23**, 056107 (2016).
- [17] M. F. F. Nave, E. Lazzaro, R. Coelho, P. Belo Abd, D. Borba, R. J. Buttery, S. N. abd F. Serra, and EFDA-JET Contributors, *Nucl. Fusion* **43**, 179 (2003).
- [18] J. L. Luxon, *Nucl. Fusion* **42**, 614 (2002).
- [19] ITER Organization, ITER Research Plan Within the Staged Approach (2018), https://www.iter.org/doc/www/content/com/Lists/ITER%20Technical%20Reports/Attachments/9/ITER-Research-Plan_final_ITR_FINAL-Cover_High-Res.pdf.
- [20] L. L. Lao, J. R. Ferron, R. J. Groebner, W. Howl, H. St. John, E. J. Strait, and T. S. Taylor, *Nucl. Fusion* **30**, 1035 (1990).
- [21] D. Wróblewski and L. L. Lao, *Rev. Sci. Instrum.* **63**, 5140 (1992).
- [22] E. J. Strait, *Rev. Sci. Instrum.* **77**, 023502 (2006).
- [23] T. N. Carlstrom, G. L. Campbell, J. C. DeBoo, R. Evanko, J. Evans, C. M. Greenfield, J. Haskovec, C. L. Hsieh, E. McKee, R. T. Snider *et al.*, *Rev. Sci. Instrum.* **63**, 4901 (1992).
- [24] S. Elgar and R. T. Guza, *Statistics of Bicoherence* (IEEE, New York, 1988), <https://doi.org/10.1109/29.7555>.
- [25] E. J. Strait, J. D. King, J. M. Hanson, and N. C. Logan, *Rev. Sci. Instrum.* **87**, 11D423 (2016).
- [26] R. Fitzpatrick, *Phys. Plasmas* **22**, 042514 (2015).
- [27] J. Wesson, *Tokamaks* (Oxford University Press, New York, 2011).
- [28] A. S. Glasser and E. Kolemen, *Phys. Plasmas* **25**, 082502 (2018).
- [29] A. S. Glasser, E. Kolemen, and A. H. Glasser, *Phys. Plasmas* **25**, 032507 (2018).
- [30] A. H. Glasser, *Phys. Plasmas* **23**, 072505 (2016).
- [31] H. P. Furth, J. Killeen, and M. N. Rosenbluth, *Phys. Fluids* **6**, 459 (1963).